Articles in PresS. Am J Physiol Cell Physiol (November 5, 2014). doi:10.1152/ajpcell.00141.2014

Cav 3.2 T-type Ca^{2+} Channels in H_2S-Mediated Hypoxic Response of the Carotid Body

Vladislav V. Makarenko, Ying-Jie Peng, Guoxiang Yuan, Aaron P. Fox, Ganesh K. Kumar, Jayasri Nanduri , and Nanduri R. Prabhakar [$]

Institute for Integrative Physiology and Center for Systems Biology of O_2 Sensing, The University of Chicago, Chicago, IL 60637

[$]To whom correspondence may be addressed. E-mail: nanduri@uchicago.edu

KEY WORDS: O_2 sensing, Voltage-gated Ca^{2+} channels, T-type Ca^{2+} channel, Carotid body, Mibefradil.

Abstract

Arterial blood oxygen (O_2) levels are detected by specialized sensory organs called carotid bodies. Voltage-gated Ca^{2+} channels (VGCC) are important for carotid body O_2 sensing. Given that T-type VGCC contributes to nociceptive sensation, we hypothesized that they participate in carotid body O_2 sensing. The rat carotid body expresses high levels of mRNA encoding α_{1H} subunit and α_{1H} protein is localized to glomus cells, the primary O_2 sensing cells in the chemoreceptor tissue suggesting that Ca_v 3.2 is the major T-Type VGCC isoform expressed in the carotid body. Mibefradil and TTA-A2, selective blockers of T-type VGCC, markedly attenuated hypoxia-evoked $[Ca^{2+}]_i$ elevation, catecholamine (CA) secretion from glomus cells and sensory excitation of the rat carotid body. Similar results were also obtained in the carotid body and glomus cells from Ca_v 3.2 knockout mice (*Cacna1h*$^{-/-}$). Since cystathionine-γ-lyase (CSE)-derived hydrogen sulfide (H_2S) is a critical mediator of carotid body response to hypoxia, the role of T-type VGCC in H_2S-mediated O_2 sensing was examined. Like hypoxia, NaHS, a H_2S donor increased $[Ca^{2+}]_i$ and augmented carotid body sensory nerve activity in wild type mice and these effects were markedly attenuated in *Cacna1h*$^{-/-}$ mice. In wild type mice, TTA-A2 markedly attenuated glomus cell and carotid body sensory nerve responses to hypoxia and these effects were absent in CSE knockout mice. These results demonstrate that Ca_v 3.2 T-type VGCC contribute to H_2S mediated carotid body response to hypoxia.

Introduction

Voltage-gated Ca^{2+} channels (VGCC) are critical for Ca^{2+} influx and neurotransmission in the nervous system (2, 13). Based on their activation properties, VGCC are divided into high- and low voltage-activated channels. High threshold VGCC are further subdivided into L-, N-, P/Q-, and R-types, while low voltage-activated Ca^{2+} channels are represented by T-type VGCC (3, 6), which are designated as Ca_V 3.1, Ca_V 3.2, and Ca_V 3.3 channels containing pore-forming α_{1G}, α_{1H}, and α_{1I} subunits, respectively (3, 29).

Carotid bodies are the sensory organs for monitoring arterial blood O_2 levels. Hypoxemia (i.e., reduced O_2 levels in blood) increases carotid body sensory nerve activity and triggers the chemosensory reflex, which is critical for maintaining cardio-respiratory functions during low O_2 (10). The carotid body is comprised of glomus (also called type I) and type II cells, and glomus cells are the primary O_2 sensing cells (10). Sensory nerve excitation by hypoxia requires elevation of $[Ca^{2+}]_i$ (1, 14, 30) and Ca^{2+}-dependent neurotransmitter(s) release from glomus cells (16, 30).

Previous studies have shown that VGCC are critical for hypoxia-evoked $[Ca^{2+}]_i$ elevation in glomus cells (10). Glomus cells express high voltage-activated Ca^{2+} currents including L-, N-, P-, and "blocker resistant" Ca^{2+} currents (7, 18, 31), and L-type VGCCs mediate a substantial portion of the hypoxia-induced Ca^{2+} influx (1, 26). Relatively little information is available on the role of T-type VGCC in the carotid body. A nickel sensitive Ca^{2+} current was reported in rat glomus cells (7). Since nickel is known to block T-type VGCC (11), this finding suggests that glomus cells also express T-type VGCC. Rat carotid body expresses mRNA encoding α_{1G} subunit and Ca_v 3.1 was proposed to contribute to hypoxia-evoked catecholamine efflux (5). However, the roles of other T-type VGCC isoforms in the carotid body response to hypoxia have not been examined.

Recent studies showed that dorsal root ganglion cells express T-type VGCC and that their activation by hydrogen sulfide (H_2S) contribute to hyperalgesia (17). Recent studies reported that

cystathionine-ϒ-lyase (CSE) generated H_2S is required for VGCC mediated $[Ca^{2+}]_i$ influx in glomus cells (14) and sensory nerve excitation of the carotid body (12, 20) . Whether H_2S is required for T-type VGCC–dependent carotid body response to hypoxia, however, is not known.

In the present study, we determined the expression and localization of T-type VGCCs in the carotid body, assessed their functional significance using pharmacological and genetic approaches, and elucidated the role of H_2S. Our results demonstrate that Ca_V 3.2 is the predominant T-type VGCC expressed in the glomus cells, which contributes to hypoxia-evoked Ca^{2+} influx, catecholamine secretion as well as sensory nerve excitation. Our results further demonstrate that CSE-derived H_2S is required for Ca_V 3.2-dependent carotid body response to hypoxia.

Methods

Experimental protocols were approved by the Institutional Animal Care and Use Committee of the University of Chicago. All experiments were performed on adult male Sprague-Dawley rats and on age as well as gender matched *Cacna1h* $^{-/-}$, *CSE*$^{-/-}$ and C57BL/6J mice.

Real-time RT-PCR

Carotid bodies were harvested from anesthetized rats (n=4 rats). Two carotid bodies were pooled and RNA was extracted using TRIZOL and was reverse transcribed using superscript III reverse transcriptase. Real-time RT-PCR was performed using a MiniOpticon system (Bio-Rad Laboratories) with SYBR GreenER two-step qRT-PCR kit (#11764–100, Invitrogen). Primer sequences for real time RT-PCR amplification were as follows: 18S forward (fw), GTAACCCGTTGAACCCCATT; 18S reverse (rev), CCATCCAATCGGTAGTAGCG (size, 151; GenBank accession number X_01117); Ca_v 3.1 fw, 5′CTTTGACCTGCTGACACTCTG; Ca_v 3.1 rev, GCCATTACAGTCTTGGT GCTCA (size, 185; GenBank accession number AF290212); Ca_v 3.2 fw, ACTTGGCCATCGTCCTCCTA; Ca_v 3.2 rev, ATGGTGGGATTGATGGGCAG (size, 101; GenBank accession number AF290213); Ca_v 3.3 fw, GACCCCA GAG CAGTGAGGAT; Ca_v 3.3 rev, TACTTGCTGTCCACGATGCC (size, 155; GenBank accession number AF 290214). Relative mRNA quantification was calculated using the comparative threshold (C_T) method using the formula "$2^{-\Delta C}{}_T$" where ΔC_T is the difference between the threshold cycle of the given target cDNA. The C_T value was taken as a fractional cycle number at which the emitted fluorescence of the sample passes a fixed threshold above the baseline. mRNA levels were normalized to 18S gene. Purity and specificity of all products were confirmed by omitting the template and by performing a standard melting curve analysis.

Immunocytochemistry

Anesthetized rats (Urethane; 1.2 g/kg, I.P.; n=4 rats) were perfused transcardially with heparinized saline followed by 4% (vol/vol) paraformaldehyde. The carotid bifurcations were dissected and immersed in 25% sucrose solution in distilled water at 4°C for 16–24 h. The tissues were mounted in OCT compound, and 8- to 10-μm-thick sagittal sections were cut and processed for immunofluorescence. The tissue sections were treated with 20% normal goat serum (NGS) and 0.2% Triton X-100 in PBS for 2 h, followed by incubation with polyclonal anti-α_{1H} (1:200 dilution; Alomone Labs; Cat # ACC-025) and monoclonal anti-tyrosine hydroxylase (TH; 1:2,000 dilution; Sigma) antibodies in PBS with 1% NGS and 0.2% Triton X-100. Control sections were treated with primary anti-α_{1H} antibody pre-incubated with α_{1H} control peptide (1:200 dilution; Alomone Labs). Immunostained regions were visualized with Alexa Red and Alexa Green (Molecular Probes) fluorescently labeled secondary antibodies. Sections mounted in Vectashield containing DAPI (Vector Labs) were analyzed using a fluorescent microscope (Eclipse E600; Nikon).

Western Blot Assay

Dorsal root ganglia were harvested from anesthetized rats (Urethane; 1.2 g/kg, I.P.), and homogenized in the buffer containing 25 mM Tris-HCl pH 7.6, 150 mM NaCl, 1% NP-40, 1% sodium deoxycholate, 0.1% SDS, 1 mM sodium orthovanadate, PMSF, and protease inhibitor cocktail. Tissue extracts containing equal amounts of proteins (1mg per ml) were separated on a 10% SDS–PAGE gel and transferred to polyvinylpyrrolidone difluoride (PVDF) membrane. Membranes were probed with primary polyclonal anti-α_{1H} antibody (1:200 dilution; Alomone Labs; Cat # ACC-025). Control membrane was probed with anti-α_{1H} antibody pre-incubated with equimolar α_{1H} control peptide (1:200 dilution) as described. The immune complexes were visualized using an enhanced chemiluminescence detection system (Amersham). The blots were scanned and quantified using Scion Image Software (NIH).

Carotid body sensory activity

The protocol for recording sensory activity from *ex vivo* carotid bodies were essentially the same as described previously (21). Briefly, the carotid body with the sinus nerve, was placed in a recording chamber (250µl volume) and superfused at a rate of 2.5 ml/min with warm (36°C) physiological saline (in mM: 125 NaCl, 5 KCl, 1.8 $CaCl_2$, 2 $MgSO_4$, 1.2 NaH_2PO_4, 25 $NaHCO_3$, 10 d-glucose, and 5 sucrose). The medium was bubbled with 21% O_2-5% CO_2. Po_2 (141 ± 2.8 mmHg), Pco_2 (35 ± 3 mmHg), and pH (7.36 ± 0.01) were determined by a blood-gas analyzer (model ABL 5, Radiometer, Copenhagen, Denmark). To facilitate recording of clearly identifiable action potentials, the sinus nerve was treated with 0.1% collagenase for 5 min. Action potentials (2–4 active units) were recorded from one of the nerve bundles with a suction electrode, amplified (AC preamplifier, 100–3,000 Hz bandwidth; model P511K, Grass Instrument), displayed on an oscilloscope (model 5B12N, Tektronix), and stored in a computer via an analog-to-digital translation board (PowerLab/8P, AD Instruments). "Single" units were selected on the basis of the height and duration of the individual action potentials using a spike discrimination program (Spike Histogram Program, PowerLab, AD Instruments).

Primary cultures of glomus cells

Preparation of primary cultures of glomus cells is essentially the same as described previously (14, 19). Briefly, carotid bodies were harvested from anesthetized rats and mice (Urethane, 1.2 g/kg, I.P.), and glomus cells were dissociated using a mixture of collagenase P (2 mg/ml; Roche.USA), DNAse (15 µg/ml; Sigma, USA), and bovine serum albumin (BSA; 3 mg/ml; Sigma, USA) at 37°C for 20 min, followed by a 15 min incubation in medium containing DNAse (30 µg/ml). Cells were plated on collagen (type VII; Sigma)-coated cover slips and maintained at 37°C in a 7% CO_2 + 20% O_2 incubator for 24 h. The growth medium consisted of F-

12K medium (Invitrogen) supplemented with 1% fetal bovine serum, insulin-transferrin-selenium (ITS-X; Invitrogen), and 1% penicillin/streptomycin/glutamine mixture (Invitrogen).

Measurements of $[Ca^{2+}]_i$

Glomus cells were incubated in Hanks Balanced Salt Solution (HBSS) with 2 μM fura-2-AM and 1 mg/ml albumin for 30 min and then washed in a fura-2-free solution for 30 min at 37°C. The cover slip was transferred to an experimental chamber for determining the changes in $[Ca^{2+}]_i$. Background fluorescence at 340 and 380 nm wavelengths were obtained from an area of the cover slip that was devoid of cells. On each cover slip, five to twelve glomus cells were selected (identified by their characteristic clustering) and individual cells were imaged. Image pairs (one at 340 and the other at 380 nm) were obtained every 2s by averaging 16 frames at each wavelength. Data were continuously collected throughout the experiment. Background fluorescence was subtracted from the individual wavelengths. The image obtained at 340 nm was divided by the 380 nm image to obtain ratiometric image. Ratios were converted to free $[Ca^{2+}]_i$ using calibration curves constructed *in vitro* by adding fura-2 (50 μM free acid) to solutions containing known concentrations of Ca^{2+} (0–2000 nM). The recording chamber was continually superfused with solution from gravity-fed reservoirs.

Measurements of catecholamine secretion

Catecholamine secretion from glomus cells was monitored by amperometry as described previously (14, 19). Briefly, recordings were made from adherent cells that were under constant perfusion with a flow rate of ~ 1.0 ml/min (chamber volume, ~ 80μl). The electrode was held at +700 mV versus a ground electrode using an NPI VA-10 amplifier to oxidize catecholamines. The amperometric signal was low-pass filtered at 2 kHz (eight-pole Bessel; Warner Instruments) and sampled into a computer at 10 kHz using a 16-bit analog-to-digital converter (National Instruments). Records with root-mean-square noise >1.0 pA were not analyzed. Amperometric

197 spike features, quantal size, and kinetic parameters were analyzed using a series of macros written
198 in Igor Pro (WaveMetrics). The number of secretory events and the amount of catecholamine
199 secreted per event were analyzed in each experiment and the data were expressed as total
200 catecholamines secreted. All experiments were performed at ambient temperature (23±2°C), and the
201 solutions had the following composition (in mM): NaCl (137.93); $CaCl_2$ (1.26), $MgCl_2.6\ H_2O$ (0.4),
202 $MgSO_4.7H_2O$ (0.49), KCl (5.33), KH_2PO_4 (0.44), $Na_2HPO_4.7H_2O$ (0.34), dextrose (5.56), and
203 HEPES (20) at pH 7.35 with an osmolarity of 300 mOsm. Control normoxic solutions were
204 equilibrated with room air (P_{O_2} ~ 146 mmHg). For challenging with hypoxia, solutions were
205 degassed and equilibrated with 1% O_2 balanced with 99% N_2 that resulted in final medium P_{O_2} of
206 ~30 mmHg as measured by blood gas analyzer.

207 *Drugs and Chemicals*

208 All stock solutions were made fresh before the experiments. Mibefradil (Sigma-Aldrich),
209 nifedipine (Sigma-Aldrich), TTA-A2 ([2-(4-cyclopropylphenyl)-N-((1R)-1-[5-[(2,2,2-
210 trifluoroethyl)oxo]-pyridin-2-yl]ethyl)acetamide]; Alomone Labs), NaHS (Sigma-Aldrich) were
211 obtained from commercial sources. Mibefradil and nifedipine stock solutions were made in HBSS.
212 TTA-A2 stock solution was made in dimethyl sulfoxide (DMSO; Sigma-Aldrich; final
213 concentration of DMSO 0.002%) and the pH of final solution was adjusted to ~7.4. Stock solutions
214 of NaHS (30 mM) were prepared in HBSS, with pH adjusted to ~7.4, and were kept on ice. Desired
215 concentrations were added to glomus cell culture plates or to the reservoirs containing medium
216 irrigating the *ex vivo* carotid body preparation.

217 *Analysis of data*

218 Average data are presented as mean ± SEM. Statistical significance was assessed by
219 Student's *t*-test for statistical comparisons between two groups and one-way ANOVA followed by
220 Tukey's test for multiple groups' comparison. $P < 0.05$ was considered significant.

Results

T-type VGCC expression in the carotid body

We first determined the expression of mRNAs encoding α_{1H}, α_{1G}, and α_{1I} subunits of T-type VGCC isoforms in the rat carotid bodies by real time quantitative PCR. Rat carotid body expressed mRNAs encoding α_{1H}, α_{1G}, and α_{1I} subunits and the abundance of α_{1H} mRNA was relatively more as compared with α_{1G} and α_{1I} ($P<0.001$; Fig. 1A). The localization of α_{1H} protein was determined by immunocytochemistry. The specificity of the anti-α_{1H} antibody was determined by western blot assay of rat dorsal root ganglion, which expresses α_{1H} (28). Immunoblot assay showed a single discrete protein band with a molecular weight corresponding to α_{1H}, and this protein was absent following pre-incubation of the antibody with the control α_{1H} peptide (Fig. 1B). Carotid body sections were stained with anti-α_{1H} and tyrosine hydroxylase (TH) antibodies, the latter served as a marker of glomus cells (32). α_{1H}-like immunoreactivity was seen predominantly in glomus cells as evidenced by its co-localization with TH-positive cells (Fig. 1C).

T-type VGCC contribute to hypoxia-evoked Ca^{2+} influx in glomus cells

Hypoxia increases Ca^{2+} influx in glomus cells (10). The role of T-type VGCC in Ca^{2+} influx by hypoxia ($P_{O_2} \sim 30$ mmHg) was determined in rat glomus cells. Changes in $[Ca^{2+}]_i$ were monitored in presence of increasing concentrations of mibefradil, a pan T-type VGCC blocker (15, 23). Hypoxia increased $[Ca^{2+}]_i$ and this effect was reduced by mibefradil in a dose-dependent manner, with a maximum response at 1 μM (49±14 % reduction; $P<0.01$; Fig. 2A). However, sodium cyanide (NaCN; 3 μM)-induced Ca^{2+} influx was unaffected by 1 μM mibefradil (Fig. 2B). However, increasing mibefradil concentration to 10 μM not only inhibited hypoxia but also NaCN-evoked Ca^{2+} influx (Fig. 2A-B), suggesting that mibefradil exerts non-selective action at concentrations higher than 1 μM. Consequently, further studies were performed with 1 μM mibefradil, which selectively affected Ca^{2+} influx evoked by hypoxia.

246 The effects of 1 μM mibefradil were completely reversed within 5 min after wash out of the
247 drug (Fig. 2C-D). The residual $[Ca^{2+}]_i$ elevation by hypoxia following mibefradil was blocked by
248 80±11 % ($P<0.01$) in presence of 5 μM nifedipine, an L-type VGCC blocker. To further establish
249 the role of T-type VGCC, we examined the effects of TTA-A2, another selective T-type VGCC
250 blocker (8, 9, 24). Based on preliminary studies, we tested the effects of 25 μM TTA-A2. As
251 shown in Figure 2E-F, TTA-A2 reversibly attenuated $[Ca^{2+}]_i$ responses to hypoxia (41±16%
252 reduction; $P<0.01$).
253
254 *T-type VGCC contribute to hypoxia-evoked catecholamine secretion and carotid body sensory*
255 *nerve activity*
256 Hypoxia releases catecholamines (CA) from glomus cells in a Ca^{2+}-dependent manner (10).
257 CA secretion from individual glomus cells was monitored by amperometry in the presence of either
258 1 μM mibefradil or 25 μM TTA-A2. Hypoxia evoked CA secretion was markedly reduced in the
259 presence of either mibefradil or TTA-A2 (Fig. 3A-D).
260 We then tested the effects of T-type VGCC blockers on the carotid body sensory nerve
261 response to hypoxia. These experiments utilized an *ex vivo* carotid body preparation to exclude
262 confounding influence of T-type VGCC blockers on blood pressure in intact rats. Hypoxia
263 increased the sensory nerve activity and this effect was markedly attenuated in presence of either
264 mibefradil (1 μM) or TTA-A2 (25 μM) in a reversible manner (Fig. 4A-D).
265
266 *Selective contribution of Ca_V 3.2 to glomus cell and carotid body response to hypoxia*
267 Since glomus cells express α_{1H}, the pore forming subunit of Cav 3.2 subtype of T-type
268 VGCC (Fig. 1), we sought to determine the selective role of Ca_V 3.2 in the carotid body response to

hypoxia. To this end, studies were performed on mice with homozygous deletion of α_{1H} allele *(Cacna1h$^{-/-}$)*, which exhibit attenuated Cav 3.2 T-type Ca^{2+} current (4).

Hypoxia-evoked $[Ca^{2+}]_i$ elevation and CA secretion were significantly reduced in *Cacna1h* null glomus cells as compared with WT controls (Fig. 5A-D). On average, $[Ca^{2+}]_i$ and CA secretory responses were attenuated by 63±14.6 % and 55 ± 4.0 %, respectively in *Cacna1h* null cells ($P< 0.01$; Fig. 5B and D). Likewise, *Cacna1h* null carotid bodies exhibited markedly attenuated sensory nerve response to hypoxia as compared with WT controls ($P<0.01$; Fig. 6A-B). However, NaCN-evoked sensory nerve excitation was comparable between *Cacna1h* null and WT carotid bodies (Fig. 6C).

H_2S is required for Ca_v 3.2–dependent carotid body response to hypoxia

Recent studies reported that CSE-derived H_2S is a critical mediator of carotid body response to hypoxia (12, 14, 20, 27). We hypothesized that Ca_v 3.2-dependent carotid body response to hypoxia requires H_2S. This possibility was tested in wild type (WT) and *Cacna1h$^{-/-}$* mice. In WT mice, NaHS, a H_2S donor, like hypoxia, increased $[Ca^{2+}]_i$ in glomus cells and carotid body sensory nerve activity, and these responses were markedly reduced in *Cacna1h* null glomus cells and carotid bodies (Fig. 7A-D). To assess the selective role of CSE-derived H_2S, studies were performed on WT and *CSE $^{-/-}$* mice. Hypoxia increased $[Ca^{2+}]_i$ in glomus cells and this response was attenuated by TTA-A2 in WT but not in CSE null glomus cells (Fig. 8A-B). To determine whether genetic deletion of CSE impaired T-type VGCC function, CSE null glomus cells were challenged with NaHS. In response to NaHS, $[Ca^{2+}]_i$ increased and this effect was inhibited by TTA-A2 in a reversible manner (Fig. 8C-D). Hypoxia-evoked carotid body sensory nerve excitation was reduced by TTA-A2 in WT, but not in CSE null carotid bodies (Fig. 9A-B).

Discussion

The results of the present study demonstrate that carotid bodies express T-Type VGCC and establish their functional significance in O_2 sensing. We found higher abundance of α_{1H} mRNA in carotid bodies from Sprague-Dawley rats as opposed to relatively high levels of α_{1G} mRNA expression in Wistar rat carotid bodies as reported previously (5). Our data further demonstrate that much of the α_{1H} protein is localized to glomus cells, the primary O_2 sensing cells in the carotid body. The following findings demonstrate the functional significance of T-type VGCC in carotid body O_2 sensing. First, mibefradil and TTA-A2, the two established blockers of T-type VGCC (15, 23, 24) effectively reduced hypoxia-induced Ca^{2+} influx in glomus cells by about ~50% and these effects were reversible and selective to hypoxia, because Ca^{2+} influx by NaCN was unaffected. Second, T-type VGCC blockers were equally effective in reducing hypoxia-evoked CA secretion from glomus cells as well as the carotid body sensory nerve excitation. Previous studies reported that L-type VGCC are the major contributors to Ca^{2+} influx by hypoxia in glomus cells (1, 14). Consistent with this possibility, we found that nifedipine, an L-type VGCC blocker, abolished nearly 80% of the residual Ca^{2+} influx by hypoxia following mibefradil. Together these observations demonstrate that hypoxia-induced voltage-gated Ca^{2+} influx in glomus cells requires both high- (L-type) and low-threshold (T-type) VGCCs.

Mice with genetic absence of α_{1H} (*Cacna1h*$^{-/-}$) exhibited markedly attenuated glomus cell responses to hypoxia as well as carotid body sensory nerve excitation by hypoxia; whereas carotid body responses to NaCN were unaltered in *Cacna1h* null mice. Furthermore, α_{1H} is predominantly expressed in glomus cells. Since α_{1H} constitutes the pore-forming subunit of Ca_v 3.2, these observations demonstrate Ca_v 3.2 as the major T-type VGCC, which contribute to hypoxia-evoked voltage-gated Ca^{2+} influx, neurotransmitter secretion and carotid body sensory nerve excitation.

316 The following observations suggest that CSE-derived H_2S is required for Ca_v 3.2-dependent
317 carotid body responses to hypoxia. First, like hypoxia, a H_2S donor, increased Ca^{2+} influx in glomus
318 cells and carotid body sensory nerve activity, and these effects were absent in *Cacna1h*$^{-/-}$ mice.
319 Second, the inhibitory effects of TTA-A2 on glomus cell and carotid body sensory nerve responses
320 were strikingly absent in CSE knockout mice. The lack of TTA-A2 effect in CSE knockout mice is
321 unlikely due to compromised Ca_v 3.2 function, because a H_2S donor still increased Ca^{2+} influx,
322 which could be attenuated by TTA-A2. We previously reported that L-type VGCC contribute in
323 part to the H_2S mediated hypoxic sensing by the carotid body (14). The current findings suggest that
324 in addition to L-type VGCC, H_2S-dependent hypoxic sensing also requires Ca_v 3.2 analogous to
325 their proposed role in nociception (17). However, the effects of CSE-derived H_2S on glomus cell
326 Ca_v 3.2 currents remain to be studied.

327 In summary, the present study employing pharmacological and genetic approaches
328 establishes a role for T-type VGCC, especially the Ca_v 3.2 in the carotid body sensory response to
329 acute hypoxia. Carotid body response to hypoxia is augmented by chronic intermittent hypoxia
330 (CIH) mimicking the O_2 saturation profiles encountered with recurrent apnea (22). Given that CIH
331 up regulates Ca_v 3.2 in adrenal medullary chromaffin cells (25), it would be of interest to examine
332 in future studies whether T-type VGCC contribute to CIH-evoked heightened hypoxic sensitivity of
333 the carotid body.

334
335 *Acknowledgements:* We would like to express our deep gratitude to Professor Solomon H. Snyder
336 and Moataz M. Gadalla of Johns Hopkins University School of Medicine for providing *CSE*$^{-/-}$ mice.
337 This research was supported by National Institutes of Health Grant HL-90554.

338
339

Author contributions: VM and NRP designed the research; VM, Y-JP, GY and JN performed the experiments and analyzed the data. APF contributed to analytical tools. VM, NRP and APF wrote the paper. G.K.K., and N.R.P. edited and revised the manuscript. The authors declare no conflict of interest.

FIGURE LEGENDS:

Fig. 1. T-type voltage-gated Ca^{2+} channel (VGCC) expression in the rat carotid body. (*A*) Real-time RT-PCR analysis of mRNAs encoding α_{1H}, α_{1G}, and α_{1I} subunits of T-type VGCC in rat carotid bodies. The values of mRNAs are normalized to 18S mRNA and expressed as fold change. Data presented are mean ± SEM from four individual experiments performed in triplicate. ***, $P< 0.001$; as compared to α_{1H}. (*B*) Immunoblots of rat dorsal root ganglion with anti-α_{1H} antibodies with (*right*) and without (*left*) α_{1H} control peptide. Arrow points to a protein band corresponding to the molecular weight of $\alpha_{1H.}$ (*C*) α_{1H} protein expression in rat carotid body glomus cells. Carotid bodies were stained with antibodies specific for α_{1H} (red) or for tyrosine hydroxylase (TH, green), a marker of glomus cells. Individual staining as well as merged images are shown. Immunostaining was performed with (*top panel*) and without (*middle panel*) α_{1H} control peptide. *Lower panels* represent enlarged (x 8) images of glomus cells enclosed in white rectangles. Scale bar represents 100 µm.

Fig. 2. T-type VGCC blockers attenuate hypoxia-induced $[Ca^{2+}]_i$ elevation in glomus cells of rat carotid body. *(A)* Dose-response of mibefradil, a blocker of T-type VGCC, on $[Ca^{2+}]_i$ response of glomus cells to hypoxia (P_{O_2} ~ 30 mmHg). Changes in $[Ca^{2+}]_i$ are expressed as $\Delta[Ca^{2+}]_i$ i.e., response to hypoxia minus baseline levels. Average data with each concentration of mibefradil is presented as mean ± SEM. **, $P< 0.01$; n.s. - not significant as compared to untreated controls. (*B*) Average data (mean ± SEM) of $[Ca^{2+}]_i$ responses to 3 µM NaCN presented as $\Delta[Ca^{2+}]_i$ i.e., response to NaCN minus baseline levels in presence of either vehicle (Veh) or mibefradil (Mib). *(C and E)* Examples of $[Ca^{2+}]_i$ responses of glomus cells to hypoxia (Hx; P_{O_2} ~ 30 mmHg) in presence of either vehicle (Veh; *C and E, left panels*) or 1 µM mibefradil (Mib; *C, middle panel*) or 25 µM TTA-A2 (TTA; *E, middle panel*), and 5 min after wash out of either mibefradil or TTA-A2 (Veh; *C and E, right panels)*. *(D and F)* Average data (mean ± SEM) of $[Ca^{2+}]_i$ responses to hypoxia

presented as $\Delta[Ca^{2+}]_i$ i.e., response to hypoxia minus baseline levels in presence of either vehicle (Veh) or 1 μM mibefradil (Mib; *D*) or 25 μM TTA-A2 (TTA; *F*). The numbers indicated within the bars of *B, D* and *F* represent number of cells used for the analyses. Horizontal bars in *C,* and *E* represent the duration of challenges with either hypoxia or vehicle or mibefradil or TTA-A2. **, $P<$ 0.01; n.s. - not significant ($P>$ 0.05) as compared to vehicle treated controls.

Fig. 3. Effect of T-type VGCC blockers on hypoxia-evoked catecholamine (CA) secretion from glomus cells. Glomus cells were isolated from carotid bodies harvested from anesthetized rats and CA secretion was monitored by amperometry. (*A and C)* Examples of hypoxia (Hx; P_{O_2} ~ 30 mmHg)-evoked CA secretion from rat glomus cells in presence of either vehicle (Veh) or 1 μM mibefradil (Mib; *A*) or 25 μM TTA-A2 (TTA; *C*). Horizontal bars represent the duration of challenges with either hypoxia or vehicle or mibefradil or TTA-A2. (*B and D)* Average data (mean ± SEM) showing the total number of CA molecules secreted during hypoxia. The numbers indicated within the bars of *B* and *D* represent the number of cells used for the analyses. **$P<$ 0.01; n.s.- not significant (P>0.05) as compared to vehicle-treated glomus cells.

Fig. 4. Effect of T-type Ca^{2+} channel blockers on carotid body sensory response to hypoxia. Carotid bodies were harvested from anesthetized rats and the sensory nerve activity was recorded ex vivo. *(A and C)* Representative examples of sensory nerve responses [impulses (imp)/s] to hypoxia (Hx; P_{O_2} ~ 30 mm Hg) in the presence of either vehicle (Veh) or 1 μM mibefradil (Mib; *A)* or 25 μM TTA-A2 (TTA; *C*) and 5 min after washout of drugs (Wash). Horizontal bars represent the duration of various challenges. *Inset*: superimposed action potentials of a "single" fiber from which data were derived. *(B and D)* Average data of the effects of 1 μM mibefradil *(*Mib; *B)* or TTA-A2 (TTA; *D)* on sensory nerve response to hypoxia presented as change (Δ) i.e., stimulus-evoked

activity minus baseline activity (imp/sec) presented as mean ± SEM. The numbers indicated within bars of *B* and *D* represent the number of experiments. ** $P< 0.01$; n.s. - not significant (P>0.05) as compared to vehicle treated controls.

Fig. 5. Glomus cell $[Ca^{2+}]_i$ and catecholamine secretory responses to hypoxia in Wild type (WT) and *Cacna1h*$^{-/-}$ mice. *(A)* Examples of $[Ca^{2+}]_i$ responses to hypoxia (Hx; $Po_2 \sim 30$ mmHg) of glomus cells from wild type (WT) and *Cacna1h*$^{-/-}$ mice. (*B*) Average data (mean ± SEM) of $[Ca^{2+}]_i$ responses to hypoxia presented as change (Δ) i.e., stimulus-evoked response minus baseline levels. *(C)* Examples of hypoxia ($Po_2 \sim 30$ mmHg)-evoked catecholamine (CA) secretion from glomus cells from WT and *Cacna1h*$^{-/-}$ mice. *(D)* Average data (mean ± SEM) showing the total number of CA molecules secreted during hypoxia. Horizontal bars in *A* and *C* represent the duration of the hypoxic challenge. The numbers indicated within the bars of *B* and *D* represent the number of cells used for analyses. **, $P< 0.01$; n.s.- not significant ($P> 0.05$) as compared to WT cells.

Fig. 6. Carotid body sensory response to hypoxia in wild type (WT) and *Cacna1h*$^{-/-}$ mice. *(A)* Representative examples of carotid body sensory nerve responses [impulses (imp)/s] to hypoxia (Hx; $Po_2 \sim 30$ mmHg) in wild type (WT) and *Cacna1h*$^{-/-}$ mice. Horizontal bars represent the duration of the hypoxic challenge. *Inset*: superimposed action potentials of a "single" fiber from which data were derived. *(B-C)* Average data (mean ± SEM) of carotid body sensory nerve response to hypoxia (*B*) or 3 μM NaCN (*C*) presented as change (Δ) i.e., stimulus-evoked activity minus baseline activity (imp/sec). The numbers shown within the bars of *B* and *C* represent the number of experiments. ** $P< 0.01$; n.s.- not significant (P>0.05) as compared to WT mice.

Fig.7. Glomus cell and carotid body responses to NaHS in wild type (WT) and *Cacna1h*$^{-/-}$ mice. *(A)* Examples of $[Ca^{2+}]_i$ responses to 50 μM NaHS and hypoxia (Hx; Po_2 ~ 30 mmHg) in glomus cells from WT and *Cacna1h*$^{-/-}$ mice. *(B)* Average data (mean ± SEM) of $[Ca^{2+}]_i$ responses to 50 μM NaHS and hypoxia in glomus cells from WT and *Cacna1h*$^{-/-}$ mice analyzed as change (Δ) i.e., stimulus-evoked response minus baseline levels. *(C)* Representative examples of carotid body sensory nerve responses [impulses (imp)/s] to 50 μM NaHS and hypoxia (Hx; Po_2 ~ 30 mmHg*)* in WT and *Cacna1h*$^{-/-}$ mice. *(D)* Average data (mean ± SEM) of carotid body sensory nerve response to NaHS or hypoxia analyzed as change (Δ) i.e., stimulus-evoked activity minus baseline activity (imp/sec). Horizontal bars in *A* and *C* represent the duration of exposure to NaHS or hypoxia. The numbers shown within bars of *B* and *D* represent the number of cells used for analyses. *(B and D)* **, $P< 0.01$; *, $P< 0.05$; n.s. - not significant ($P> 0.05$) as compared to WT.

Fig.8. Effect of TTA-A2 on $[Ca^{2+}]_i$ responses of glomus cells to hypoxia and H_2S in wild type (WT) and *CSE*$^{-/-}$ mice. *(A and C)* Examples of $[Ca^{2+}]_i$ responses to hypoxia *(A)* or 50 μM NaHS *(C)* in the presence of either vehicle (Veh) or 25 μM TTA-A2 (TTA) in glomus cells from WT and *CSE*$^{-/-}$ mice. Horizontal bars in *A* and *C* represent the duration of exposure to various challenges including NaHS, hypoxia, vehicle, and TTA-A2. *(B and D)* Average data (mean ± SEM) of $[Ca^{2+}]_i$ responses to either hypoxia *(B)* or 50 μM NaHS *(D)* in glomus cells from WT and *CSE*$^{-/-}$ mice presented as change (Δ) i.e., stimulus-evoked response minus baseline levels. The numbers shown within the bars of *B* and *D* represent the number of cells used for analyses. **, $P< 0.01$; n.s. - not significant ($P> 0.05$) as compared to vehicle treated cells.

Fig. 9. Effect of TTA-A2 on carotid body sensory nerve responses to hypoxia in WT and *CSE*$^{-/-}$ mice. *(A)* Representative examples of sensory nerve responses [impulses (imp)/s] to hypoxia (Hx;

442 P_{O_2} ~ 30 mmHg*)* in WT and $CSE^{-/-}$ mice in presence of either vehicle (Veh) or TTA-2A (TTA).
443 Horizontal bars represent the duration of hypoxia challenge, vehicle or TTA-A2. *Inset*:
444 superimposed action potentials of a "single" fiber from which data were derived. *(B)* Average data
445 (mean ± SEM) of carotid body sensory response to hypoxia analyzed as change (Δ) i.e., stimulus-
446 evoked activity minus baseline activity (imp/sec). The numbers shown within the bars represent the
447 number of experiments. ** $P< 0.01$; n.s. - not significant ($P> 0.05$) as compared to vehicle-treated
448 control.

REFERENCES:

1. **Buckler KJ, and Vaughan-Jones RD**. Effects of hypoxia on membrane potential and intracellular calcium in rat neonatal carotid body type I cells. *J Physiol* 476: 423-428, 1994.

2. **Catterall WA**. Voltage-gated calcium channels. *Cold Spring Harb Perspect Biol* 3: a003947, 2011.

3. **Catterall WA, Perez-Reyes E, Snutch TP, and Striessnig J**. International Union of Pharmacology. XLVIII. Nomenclature and structure-function relationships of voltage-gated calcium channels. *Pharmacol Rev* 57: 411-425, 2005.

4. **Chen CC, Lamping KG, Nuno DW, Barresi R, Prouty SJ, Lavoie JL, Cribbs LL, England SK, Sigmund CD, Weiss RM, Williamson RA, Hill JA, and Campbell KP**. Abnormal coronary function in mice deficient in alpha1H T-type Ca2+ channels. *Science* 302: 1416-1418, 2003.

5. **Cáceres AI, Gonzalez-Obeso E, Gonzalez C, and Rocher A**. RT-PCR and pharmacological analysis of L-and T-type calcium channels in rat carotid body. *Adv Exp Med Biol* 648: 105-112, 2009.

6. **Dolphin AC**. Calcium channel diversity: multiple roles of calcium channel subunits. *Curr Opin Neurobiol* 19: 237-244, 2009.

7. **e Silva MJ, and Lewis DL**. L- and N-type Ca2+ channels in adult rat carotid body chemoreceptor type I cells. *J Physiol* 489 (Pt 3): 689-699, 1995.

8. **Francois A, Kerckhove N, Meleine M, Alloui A, Barrere C, Gelot A, Uebele VN, Renger JJ, Eschalier A, Ardid D, and Bourinet E**. State-dependent properties of a new T-type calcium channel blocker enhance Ca(V)3.2 selectivity and support analgesic effects. *Pain* 154: 283-293, 2013.

9. **Kraus RL, Li Y, Gregan Y, Gotter AL, Uebele VN, Fox SV, Doran SM, Barrow JC, Yang ZQ, Reger TS, Koblan KS, and Renger JJ**. In vitro characterization of T-type calcium channel antagonist TTA-A2 and in vivo effects on arousal in mice. *J Pharmacol Exp Ther* 335: 409-417, 2010.

10. **Kumar P, and Prabhakar NR**. Peripheral Chemoreceptors: Function and Plasticity of the Carotid Body. Compr Physiol, 2012, p. 141-219.

11. **Lee JH, Gomora JC, Cribbs LL, and Perez-Reyes E**. Nickel block of three cloned T-type calcium channels: low concentrations selectively block alpha1H. *Biophys J* 77: 3034-3042, 1999.

12. **Li Q, Sun BY, Wang XF, Jin Z, Zhou Y, Dong L, Jiang LH, and Rong WF**. A Crucial Role for Hydrogen Sulfide in Oxygen Sensing via Modulating Large Conductance Calcium-Activated Potassium Channels. *Antioxidants & Redox Signaling* 12: 1179-1189, 2010.

13. **Lipscombe D, Allen SE, and Toro CP**. Control of neuronal voltage-gated calcium ion channels from RNA to protein. *Trends Neurosci* 36: 598-609, 2013.

14. **Makarenko VV, Nanduri J, Raghuraman G, Fox AP, Gadalla MM, Kumar GK, Snyder SH, and Prabhakar NR**. Endogenous H2S is required for hypoxic sensing by carotid body glomus cells. *Am J Physiol Cell Physiol* 303: C916-C923, 2012.

15. **Martin RL, Lee JH, Cribbs LL, Perez-Reyes E, and Hanck DA**. Mibefradil block of cloned T-type calcium channels. *J Pharmacol Exp Ther* 295: 302-308, 2000.

16. **Obeso A, Rocher A, Fidone S, and Gonzalez C**. The role of dihydropyridine-sensitive Ca2+ channels in stimulus-evoked catecholamine release from chemoreceptor cells of the carotid body. *Neuroscience* 47: 463-472, 1992.

17. **Okubo K, Takahashi T, Sekiguchi F, Kanaoka D, Matsunami M, Ohkubo T, Yamazaki J, Fukushima N, Yoshida S, and Kawabata A**. Inhibition of T-type calcium channels and hydrogen sulfide-forming enzyme reverses paclitaxel-evoked neuropathic hyperalgesia in rats. *Neuroscience* 188: 148-156, 2011.

18. **Overholt JL, and Prabhakar NR**. Ca2+ current in rabbit carotid body glomus cells is conducted by multiple types of high-voltage-activated Ca2+ channels. *J Neurophysiol* 78: 2467-2474, 1997.

19. **Peng YJ, Makarenko VV, Nanduri J, Vasavda C, Raghuraman G, Yuan G, Gadalla MM, Kumar GK, Snyder SH, and Prabhakar NR**. Inherent variations in CO-H2S-mediated carotid body O2 sensing mediate hypertension and pulmonary edema. *Proc Natl Acad Sci U S A* 111: 1174-1179, 2014.

20. **Peng YJ, Nanduri J, Raghuraman G, Souvannakitti D, Gadalla MM, Kumar GK, Snyder SH, and Prabhakar NR**. H2S mediates O2 sensing in the carotid body. *Proc Natl Acad Sci U S A* 107: 10719-10724, 2010.

21. **Peng YJ, Nanduri J, Yuan G, Wang N, Deneris E, Pendyala S, Natarajan V, Kumar GK, and Prabhakar NR**. NADPH oxidase is required for the sensory plasticity of the carotid body by chronic intermittent hypoxia. *J Neurosci* 29: 4903-4910, 2009.

22. **Prabhakar NR, Fields RD, Baker T, and Fletcher EC**. Intermittent hypoxia: cell to system. *Am J Physiol Lung Cell Mol Physiol* 281: L524-L528, 2001.

513 23. **Randall AD, and Tsien RW**. Contrasting biophysical and pharmacological properties of T-
514 type and R-type calcium channels. *Neuropharmacology* 36: 879-893, 1997.
515 24. **Shipe WD, Barrow JC, Yang ZQ, Lindsley CW, Yang FV, Schlegel KA, Shu Y, Rittle**
516 **KE, Bock MG, Hartman GD, Tang C, Ballard JE, Kuo Y, Adarayan ED, Prueksaritanont T,**
517 **Zrada MM, Uebele VN, Nuss CE, Connolly TM, Doran SM, Fox SV, Kraus RL, Marino MJ,**
518 **Graufelds VK, Vargas HM, Bunting PB, Hasbun-Manning M, Evans RM, Koblan KS, and**
519 **Renger JJ**. Design, synthesis, and evaluation of a novel 4-aminomethyl-4-fluoropiperidine as a T-
520 type Ca2+ channel antagonist. *J Med Chem* 51: 3692-3695, 2008.
521 25. **Souvannakitti D, Nanduri J, Yuan G, Kumar GK, Fox AP, and Prabhakar NR**.
522 NADPH oxidase-dependent regulation of T-type Ca2+ channels and ryanodine receptors mediate
523 the augmented exocytosis of catecholamines from intermittent hypoxia-treated neonatal rat
524 chromaffin cells. *J Neurosci* 30: 10763-10772, 2010.
525 26. **Summers BA, Overholt JL, and Prabhakar NR**. Augmentation of L-type calcium current
526 by hypoxia in rabbit carotid body glomus cells: evidence for a PKC-sensitive pathway. *J*
527 *Neurophysiol* 84: 1636-1644, 2000.
528 27. **Telezhkin V, Brazier SP, Cayzac S, Müller CT, Riccardi D, and Kemp PJ**. Hydrogen
529 sulfide inhibits human BK(Ca) channels. *Adv Exp Med Biol* 648: 65-72, 2009.
530 28. **Todorovic SM, and Jevtovic-Todorovic V**. Neuropathic pain: role for presynaptic T-type
531 channels in nociceptive signaling. *Pflugers Arch* 465: 921-927, 2013.
532 29. **Tsien RW, Lipscombe D, Madison DV, Bley KR, and Fox AP**. Multiple types of neuronal
533 calcium channels and their selective modulation. *Trends Neurosci* 11: 431-438, 1988.
534 30. **Ureña J, Fernández-Chacón R, Benot AR, Alvarez de Toledo GA, and López-Barneo J**.
535 Hypoxia induces voltage-dependent Ca2+ entry and quantal dopamine secretion in carotid body
536 glomus cells. *Proc Natl Acad Sci U S A* 91: 10208-10211, 1994.
537 31. **Ureña J, López-López J, González C, and López-Barneo J**. Ionic currents in dispersed
538 chemoreceptor cells of the mammalian carotid body. *J Gen Physiol* 93: 979-999, 1989.
539 32. **Yuan G, Peng YJ, Reddy VD, Makarenko VV, Nanduri J, Khan SA, Garcia JA,**
540 **Kumar GK, Semenza GL, and Prabhakar NR**. Mutual antagonism between hypoxia-inducible
541 factors 1α and 2α regulates oxygen sensing and cardio-respiratory homeostasis. *Proc Natl Acad Sci*
542 *U S A* 110: 1788-1796, 2013.
543

Fig. 1

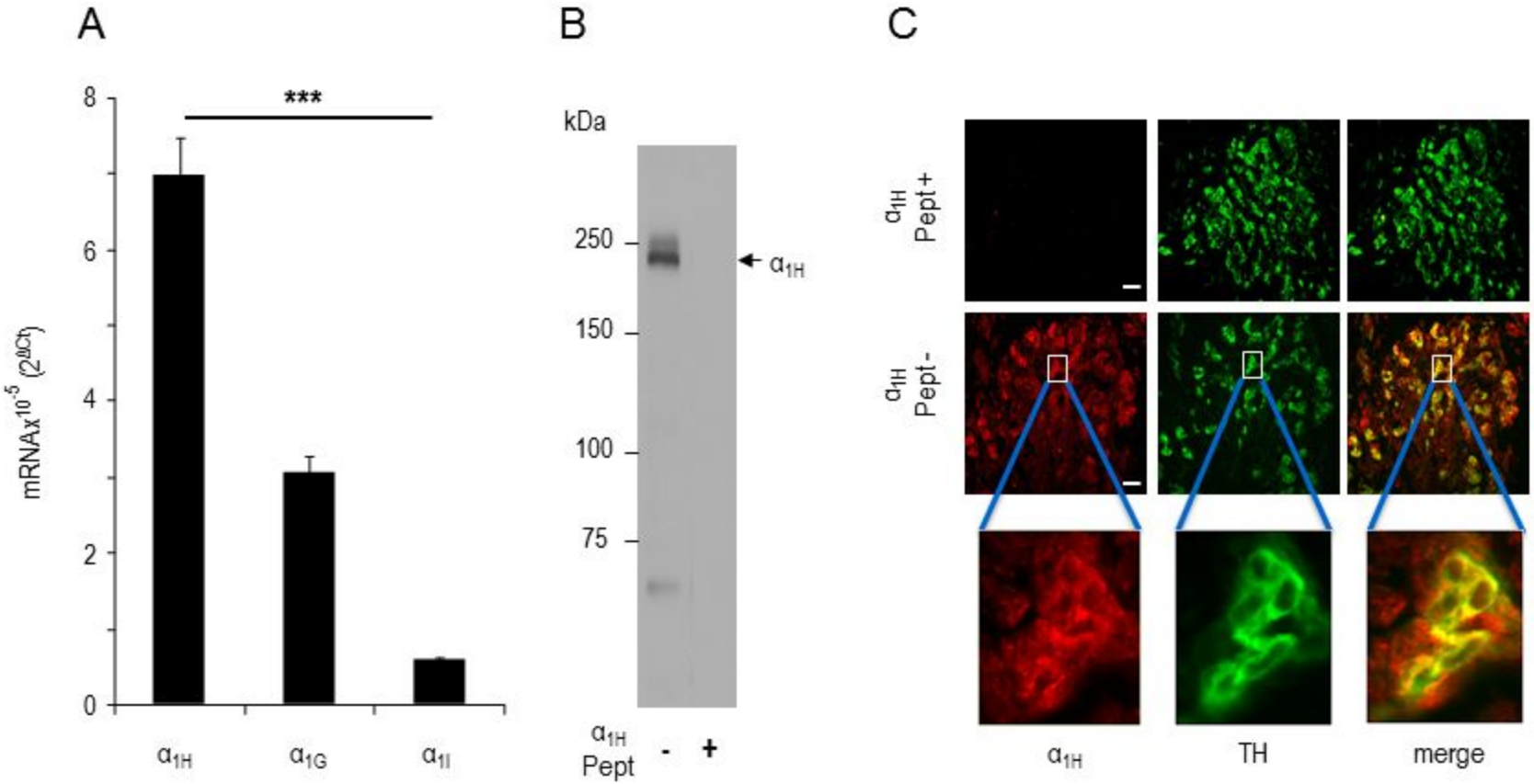
A
B
C
***
8
6
4
2
0
mRNAx10-5 (2^ΔCt)
α1H
α1G
α1I
kDa
250
150
100
75
α1H
α1H Pept - +
α1H Pept+
α1H Pept-
α1H
TH
merge

Fig. 2

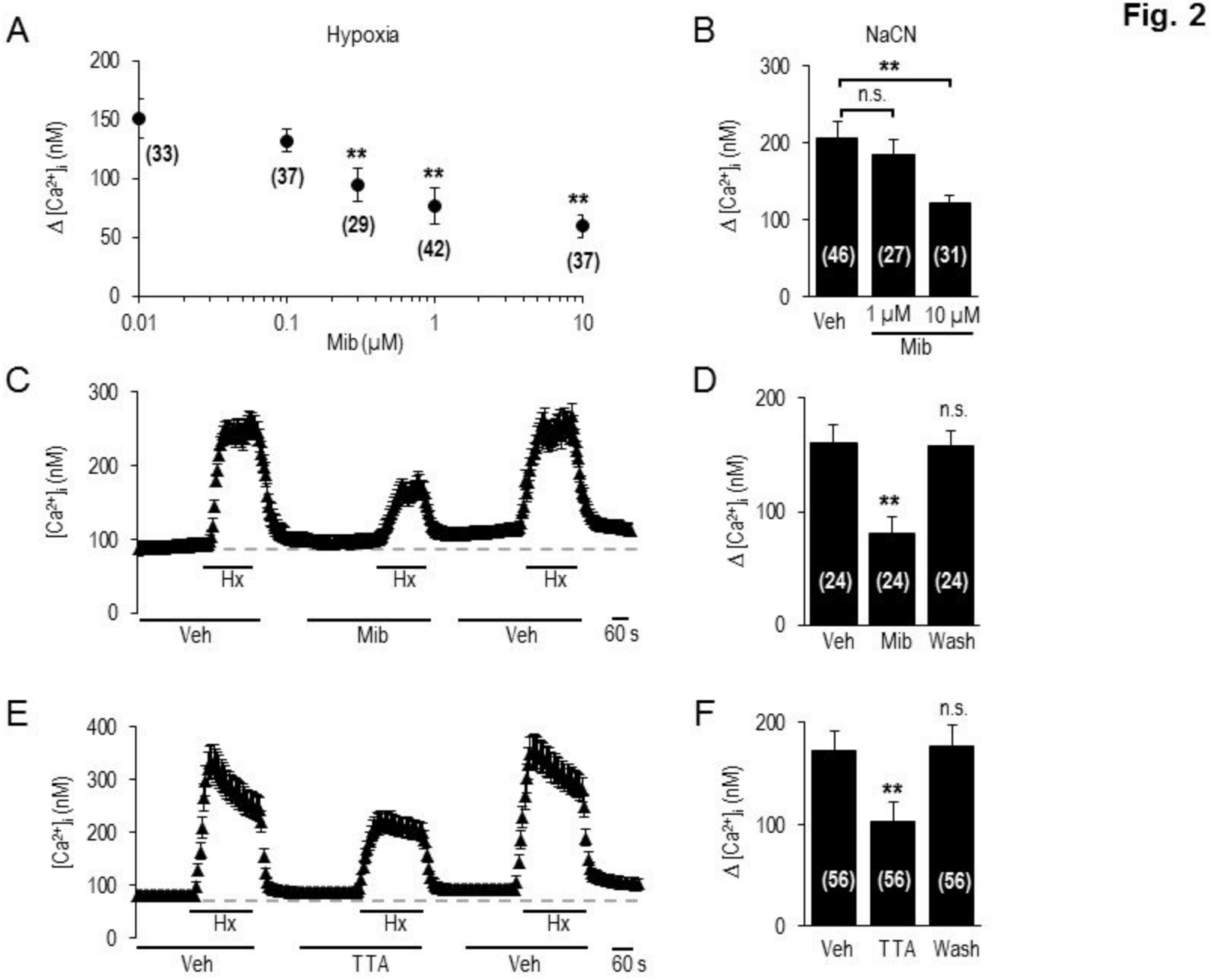
A
Hypoxia
Δ [Ca2+]i (nM)
Mib (μM)
(33)
(37)
(29)
(42)
(37)
**
B
NaCN
n.s.
(46)
(27)
(31)
Veh
1 μM
10 μM
Mib
C
[Ca2+]i (nM)
Hx
Veh
Mib
60 s
D
n.s.
(24)
Wash
E
TTA
F
(56)

Fig. 3

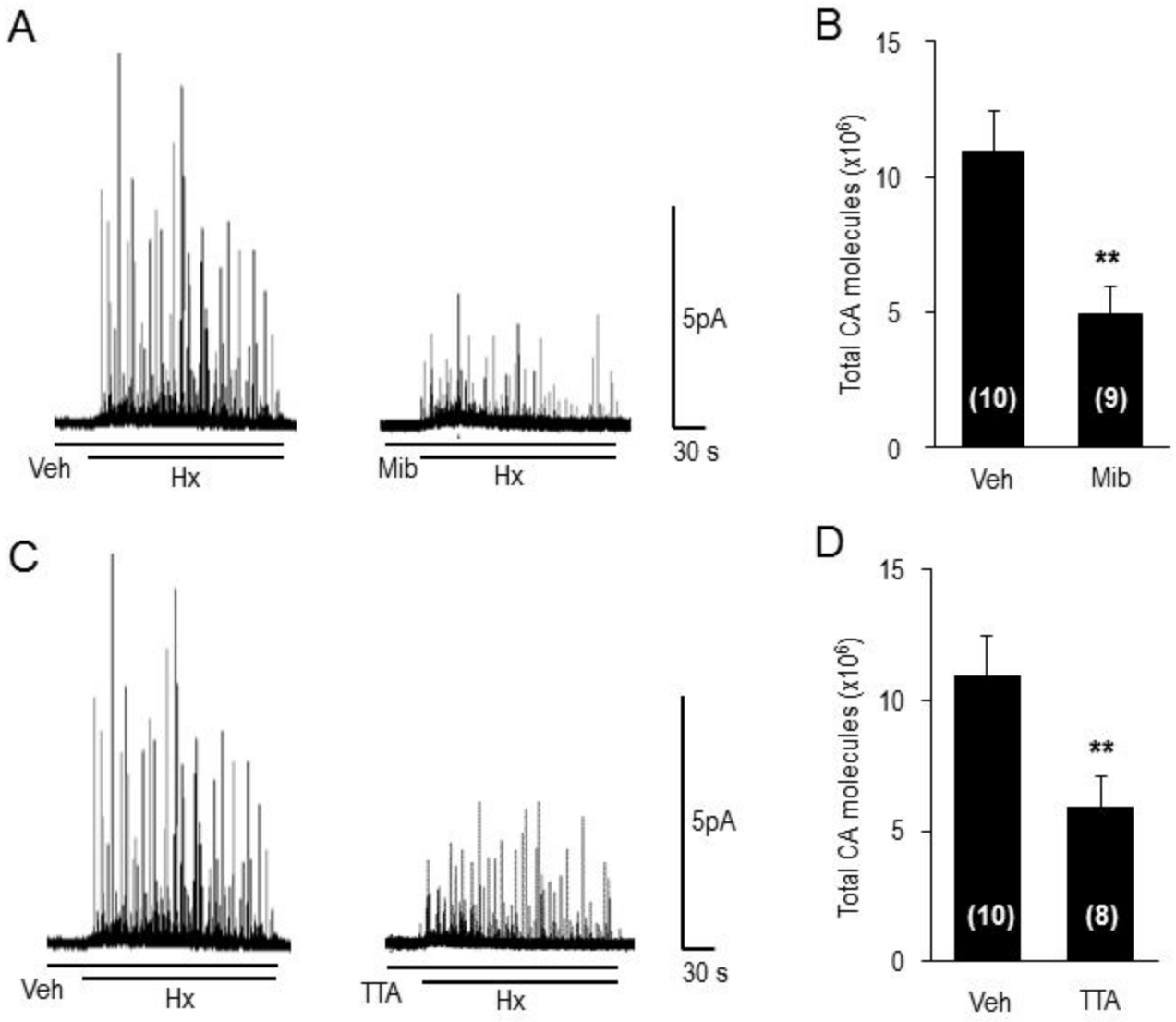
A
Veh
Hx
Mib
Hx
5pA
30 s
B
Total CA molecules (x10^6)
15
10
5
0
**
(10)
(9)
Veh
Mib
C
Veh
Hx
TTA
Hx
5pA
30 s
D
Total CA molecules (x10^6)
15
10
5
0
**
(10)
(8)
Veh
TTA

Fig. 4

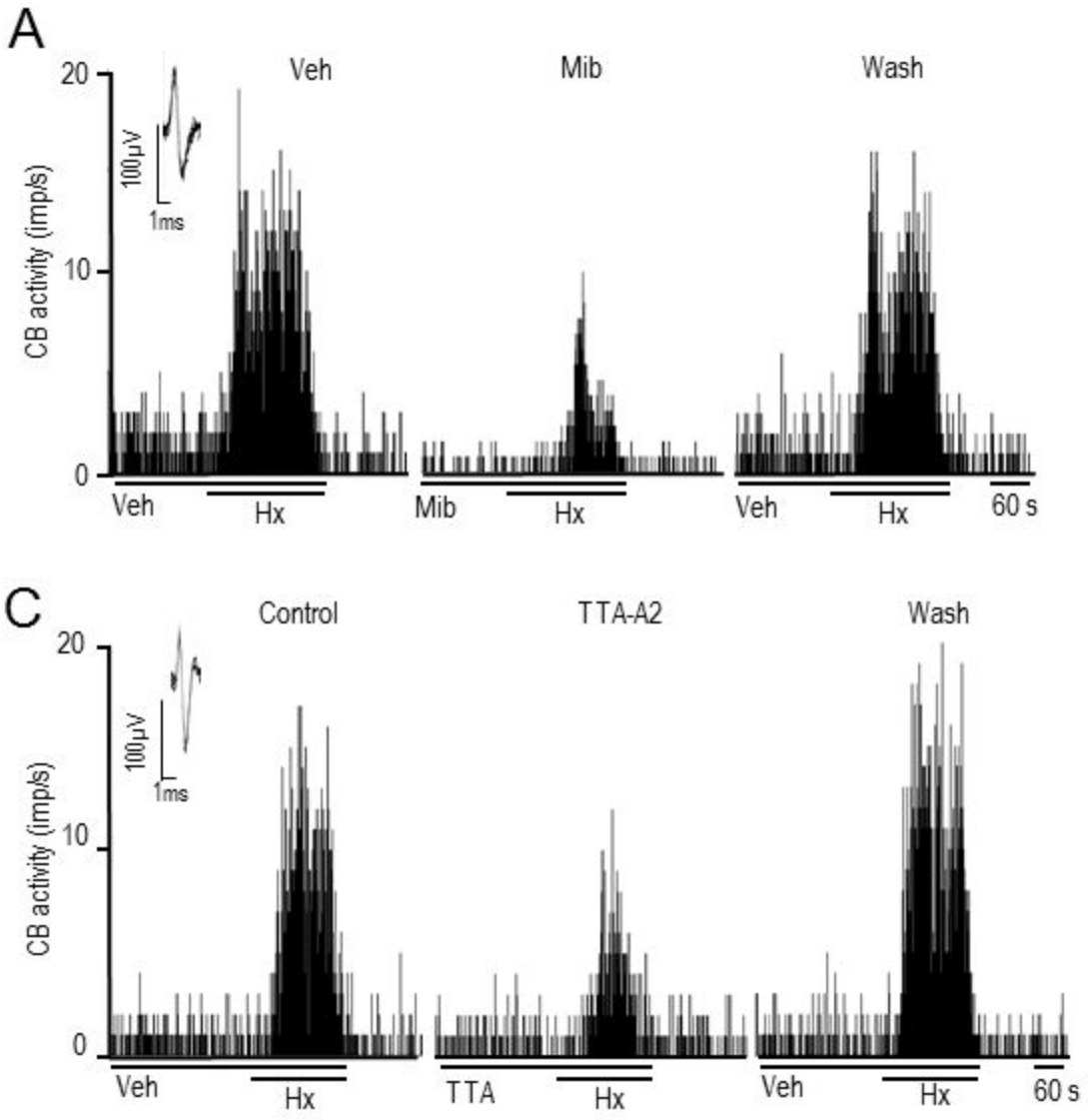
A
Veh
Mib
Wash
20
10
0
CB activity (imp/s)
100µV
1ms
Veh
Hx
Mib
Hx
Veh
Hx
60 s
B
9
6
3
0
CB response to hypoxia (Δimp/s)
n.s.
**
(10)
(10)
(10)
Veh
Mib
Wash
C
Control
TTA-A2
Wash
20
10
0
CB activity (imp/s)
100µV
1ms
Veh
Hx
TTA
Hx
Veh
Hx
60 s
D
9
6
3
0
CB response to hypoxia (Δimp/s)
n.s.
**
(11)
(11)
(11)
Veh
TTA
Wash

Fig. 5

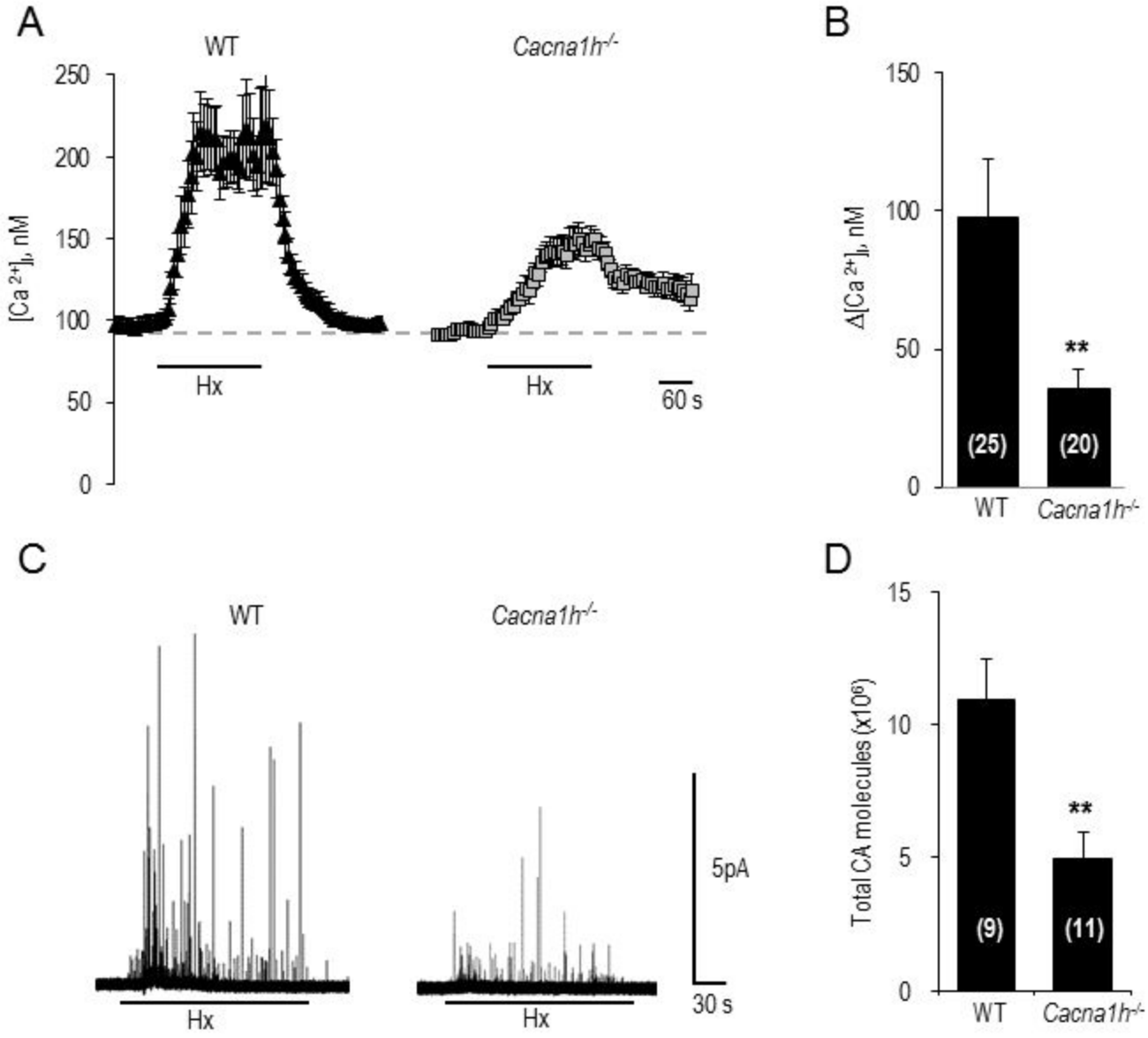
A
WT
Cacna1h-/-
250
200
150
100
50
0
[Ca 2+]i, nM
Hx
Hx
60 s
B
150
100
50
0
Δ[Ca 2+]i, nM
**
(25)
(20)
WT
Cacna1h-/-
C
WT
Cacna1h-/-
5pA
30 s
Hx
Hx
D
15
10
5
0
Total CA molecules (x10^6)
**
(9)
(11)
WT
Cacna1h-/-

Fig. 6

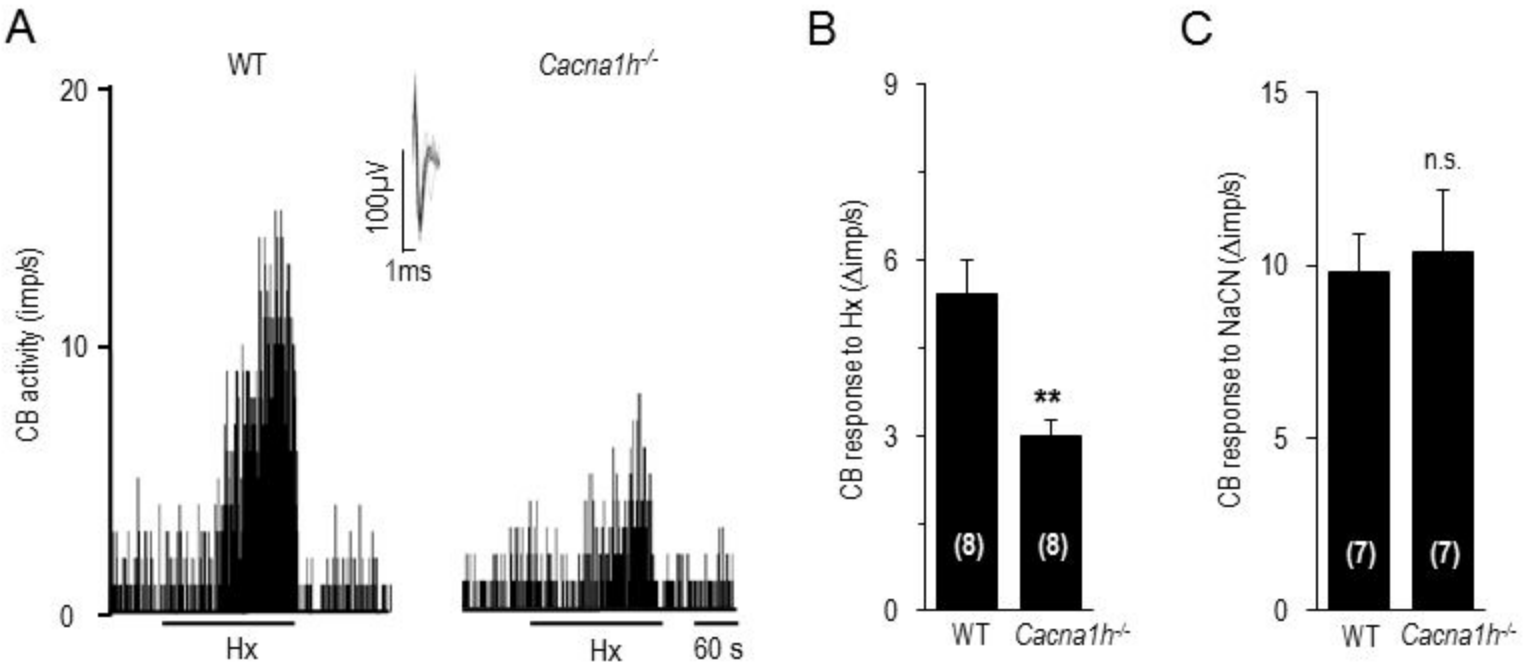
A
WT
Cacna1h-/-
20
10
0
CB activity (imp/s)
100μV
1ms
Hx
Hx
60 s
B
9
6
3
0
CB response to Hx (Δimp/s)
**
(8)
(8)
WT
Cacna1h-/-
C
15
10
5
0
CB response to NaCN (Δimp/s)
n.s.
(7)
(7)
WT
Cacna1h-/-

Fig. 7

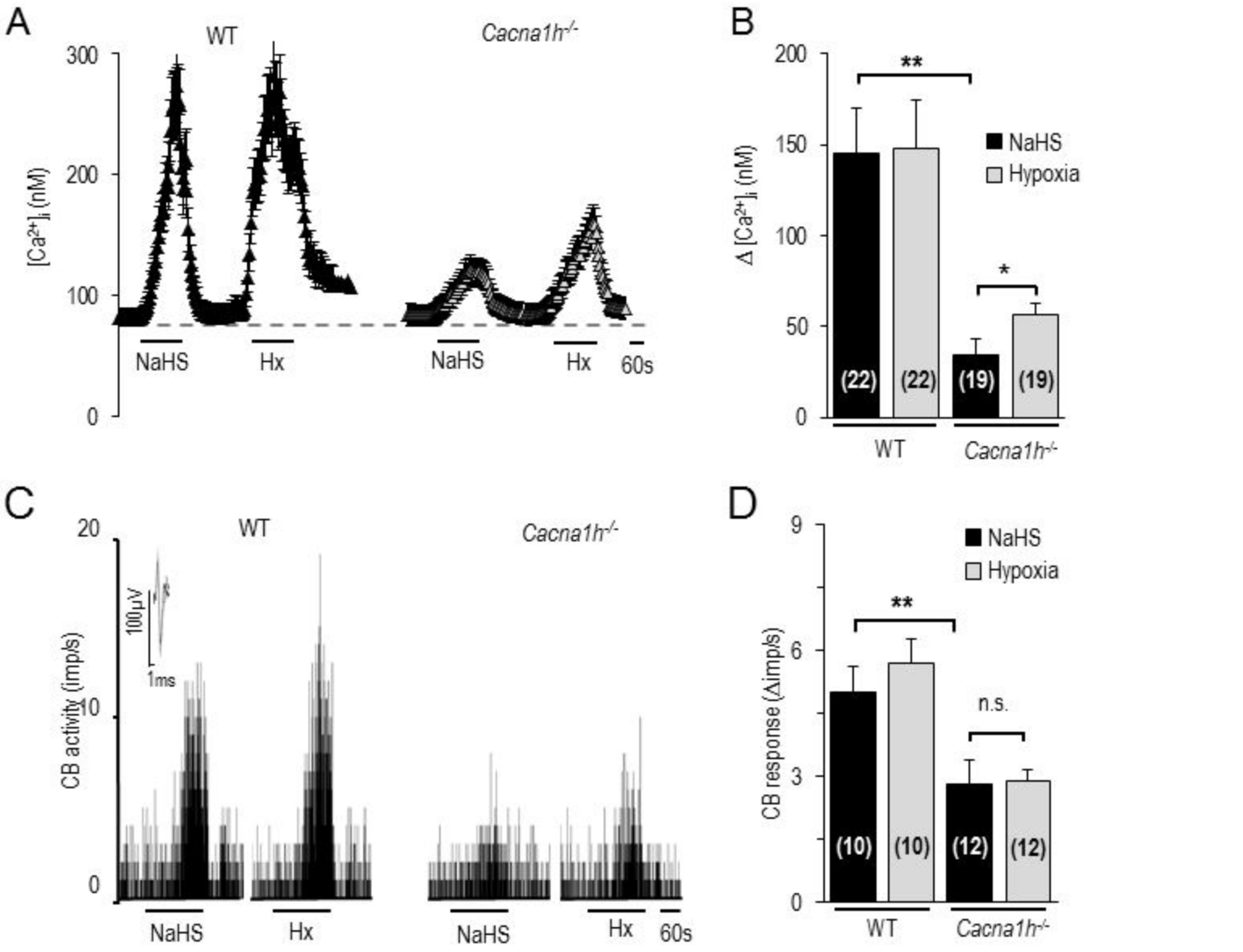
A
WT
Cacna1h-/-
300
200
100
0
[Ca2+]i (nM)
NaHS
Hx
NaHS
Hx
60s
B
200
150
100
50
0
Δ [Ca2+]i (nM)
**
*
NaHS
Hypoxia
(22)
(22)
(19)
(19)
WT
Cacna1h-/-
C
20
10
0
CB activity (imp/s)
WT
Cacna1h-/-
100μV
1ms
NaHS
Hx
NaHS
Hx
60s
D
9
6
3
0
CB response (Δimp/s)
**
n.s.
NaHS
Hypoxia
(10)
(10)
(12)
(12)
WT
Cacna1h-/-

Fig. 8

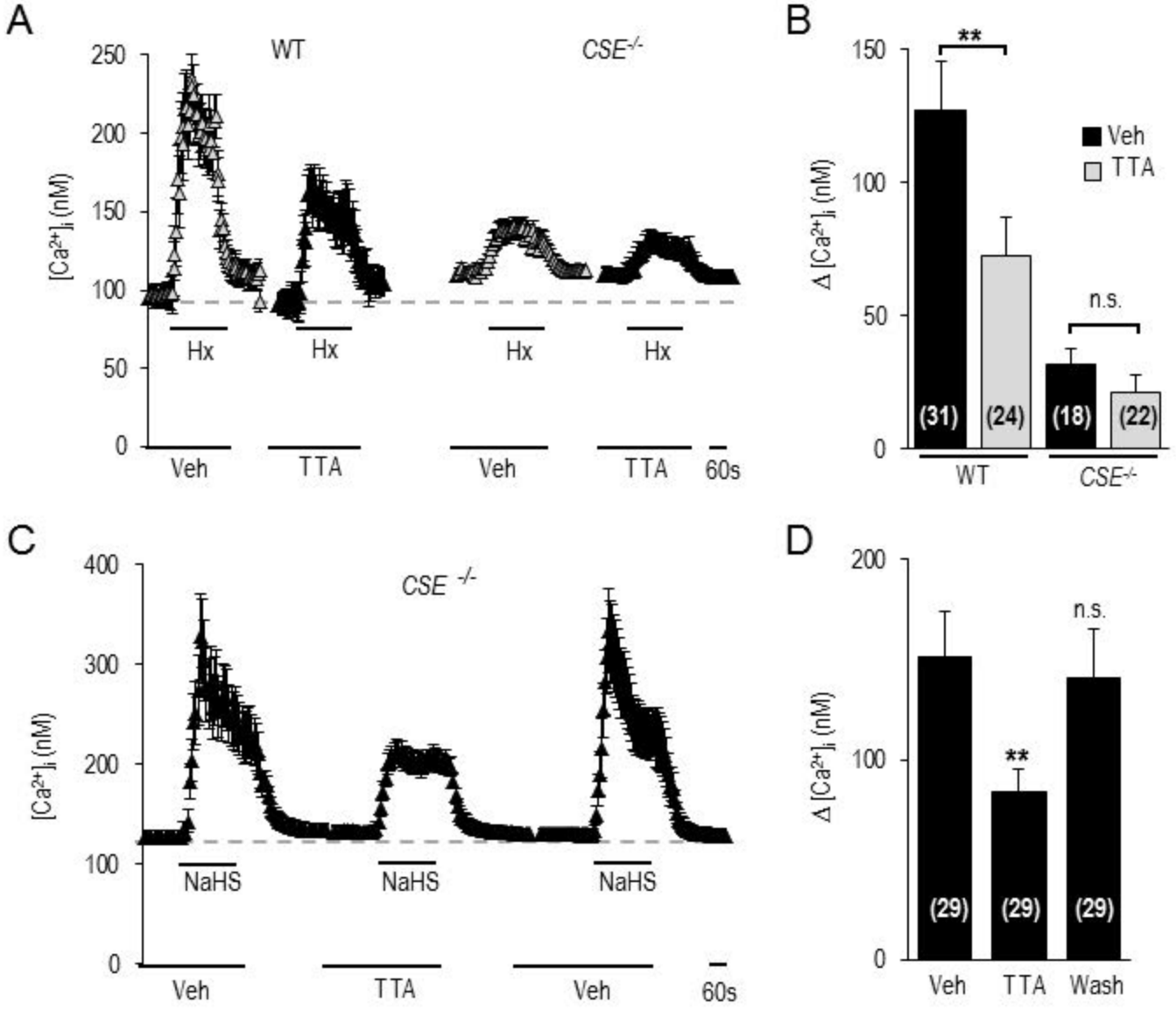
A
WT
CSE-/-
[Ca2+]i (nM)
250
200
150
100
50
0
Hx
Hx
Hx
Hx
Veh
TTA
Veh
TTA
60s
B
Δ [Ca2+]i (nM)
150
100
50
0
**
n.s.
Veh
TTA
(31)
(24)
(18)
(22)
WT
CSE-/-
C
CSE -/-
[Ca2+]i (nM)
400
300
200
100
0
NaHS
NaHS
NaHS
Veh
TTA
Veh
60s
D
Δ [Ca2+]i (nM)
200
100
0
n.s.
**
(29)
(29)
(29)
Veh
TTA
Wash

Fig. 9

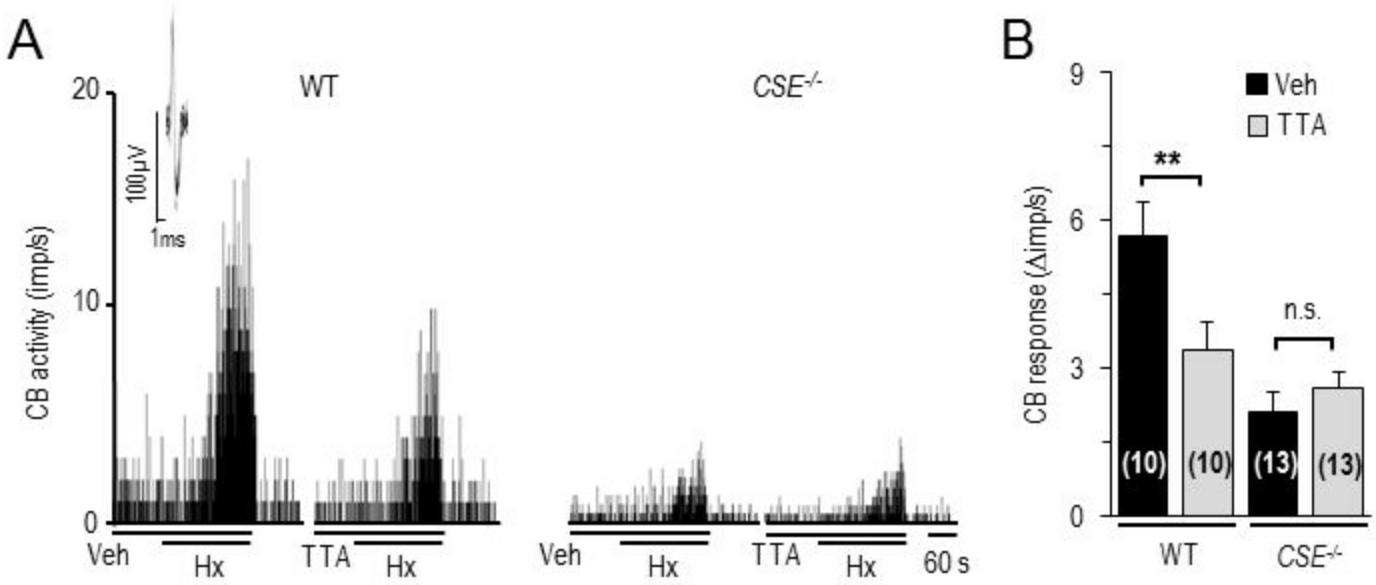
A
WT
CSE-/-
20
10
0
CB activity (imp/s)
100µV
1ms
Veh
Hx
TTA
Hx
Veh
Hx
TTA
Hx
60 s
B
9
6
3
0
CB response (Δimp/s)
Veh
TTA
**
n.s.
(10)
(10)
(13)
(13)
WT
CSE-/-